

Comparison of data approximation methods used in MR-based tissue electrical property mapping – a simulation study

Selaka Bulumulla¹, Seung-kyun Lee¹, and Ileana Hancu¹
¹GE Global Research, Niskayuna, NY, United States

Target audience: Research personnel interested in methods to image conductivity and permittivity using magnetic resonance imaging

Purpose: Calculation of electrical properties from B1+ maps is a potentially powerful method for non-invasive imaging of conductivity and permittivity. The method accurately calculates conductivity and permittivity when complex B1+ maps are available in the region of interest¹. Since B1+ phase is not directly available in an MRI scan with conventional hardware, various approximation schemes have been proposed²⁻⁵. In this work we compare four such methods in terms of accuracy of electrical property calculation using analytical and numerical simulation models.

Methods: All the methods considered here can be interpreted as the electrical properties being calculated from the Laplacian of a complex quantity through $(\nabla^2 B)/B = -\mu\epsilon_r\epsilon_0\omega^2 + i\mu\sigma\omega$, where ϵ_r and σ are the relative permittivity and conductivity to be measured, respectively. The quantity B, which is ideally the complex B1+ map, is approximated differently in different methods as summarized in Table 1. All

Method	Magnitude of B	Phase of B
1 (ideal)	$ B_1^+ $	$\angle B_1^+$
2 (ref 2,3)	$ B_1^+ $	$\phi_{TR}/2$
3 (ref 4)	$ B_1^+ $	0
4 (ref 4)	1	$\phi_{TR}/2$
5 (ref 5)	$\text{sqrt}(B_1^+ B_1^-)$	$\phi_{TR}/2$

Table 1. Definition of different methods considered. Transceiver phase ϕ_{TR} is the phase of the product $B_1^+ B_1^-$.

quantities in Methods 2-5 are MR-measurable. In particular, the transceiver phase ϕ_{TR} can be equated to the spin echo image phase. Methods 4-5 do not require dedicated B1+ mapping⁴. In Method 5, the amplitude of the product of B1+ and B1- can be obtained from a low-flip-angle gradient echo image with minimized relaxation contrast^{5,6}. Our comparative investigation consisted of simulating complex, 3-dimensional B1+ and B1- maps for a transmit-receive birdcage coil applied to three models (infinite cylinder, human head, and torso/breast model), and for each model computing ϵ_r and σ according to Table 1. All comparisons were done at 128MHz (3.0 T).

Infinite cylinder A 10 cm-diameter uniform cylinder with three different pairs of (ϵ_r, σ) was simulated. The B1+, B1- fields were calculated analytically⁷ in the axial cross section.

Human head model For this and the following models, B1+, B1- fields were simulated using HFSS (ANSYS, PA, USA). Only

Methods 1, 2, 5 were compared. The head model had two compartments, brain and muscle (outer layer).

Torso/breast geometrical model This was a geometrical model with two compartments, torso and breasts.

Results: Figure 1 shows that for a highly symmetric case of a uniform cylinder, Methods 2, 5 produce the same electrical properties as does the ideal case (Method 1). The magnitude-only and phase-only methods performed poorly for the cases of $(\epsilon_r, \sigma) = (50, 0.5)$ and $(\epsilon_r, \sigma) = (90, 0.9)$. Table 2 summarizes calculated average electrical properties in different tissue compartments in head and torso/breast models. Methods 2 and 5 perform similarly for head, but shows significant difference for the torso/breast model. Compared with the ideal case (Method 1), Method 5 works better to produce more accurate average ϵ_r and σ in the case of the torso/breast model, specifically in left/right breasts. Comparison of results between Methods 1 and 5 are shown in Fig. 2.

Discussion: Noise-free simulation as is reported here represents the first step towards more comprehensive comparison of different methods of data acquisition for MR-based electrical property mapping. We found that, when applied to noise- and contrast-free simulation models, the square-root-image-based method⁵ (Method 5) performed well, in the case of rotational symmetric model in the axial plane as well as rotationally asymmetric model (torso/breast). Sensitivity to noise, image artifacts and contrast will be the subject of future investigation.

Conclusion: Out of the several data acquisition methods considered, use of $\text{sqrt}(|B_1^+ B_1^-|)$, which may be obtained from a low flip angle gradient echo image and transceiver phase, appears to be a promising method to estimate conductivity and permittivity.

Acknowledgement: This work was supported in part by the NIH grant 1R01CA154433-01A1.

References: [1] Bulumulla S. et al, Proc ISMRM 17 (2009), 3043 [2] Katscher U. et al, IEEE Trans Med Imaging 28:1365 (2009) [3] Bulumulla S. et al, Concepts Magn Reson 41B:13 (2012) [4] Voigt T. et al, MRM 66:456 (2011) [5] Lee S-K. et al, ISMRM 2013 submitted [6] Wang J. et al, MRM 53:408 (2005) [7] Glover G. et al, JMR 64:255 (1985)

Acknowledgement: This work was supported in part by the NIH grant 1R01CA154433-01A1.

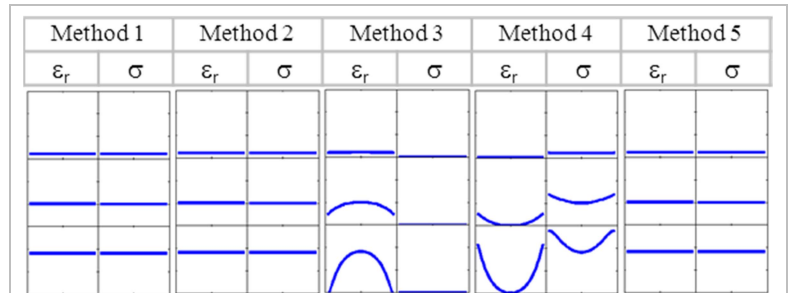


Figure 1. Electrical properties calculated for an infinite cylinder displayed along a diagonal line. All properties are axi-symmetric. The horizontal axis for each subfigure runs from -5 to 5 [cm]. The vertical axes for ϵ_r and σ run from 0 to 150, and 0 to 1.5 [S/m], respectively. All scales are linear. True parameters are: top row, $(\epsilon_r, \sigma) = (10, 0.1)$; center row, $(\epsilon_r, \sigma) = (50, 0.5)$; bottom row, $(\epsilon_r, \sigma) = (90, 0.9)$.

Tissue	Model	Method 1		Method 2		Method 5		
		ϵ_r	σ	ϵ_r	σ	ϵ_r	σ	
brain	68	0.54	65.9	0.58	65.8	0.58	65.8	0.57
outer layer	64	0.74	59.9	0.75	59.5	0.76	59.6	0.75
torso	45	0.50	43.6	0.50	44.9	0.51	42.6	0.50
breast	10/	0.15/	10.1/	0.15/	11.9/	0.18/	9.6/	0.16/
	10	0.15	10.1	0.15	5.9	0.14	9.6	0.16

Table 2. Electrical properties from simulated B1+ maps in head and torso/breast models

Method 5 works better to produce more accurate average ϵ_r and σ in the case of the torso/breast model, specifically in left/right breasts. Comparison of results between Methods 1 and 5 are shown in Fig. 2.

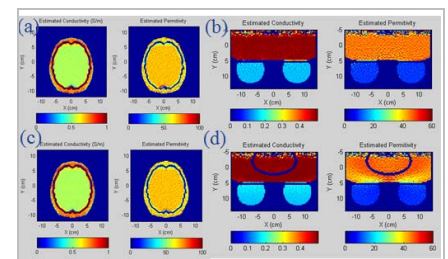


Figure 2. Conductivity [S/m] (left) and relative permittivity (right) maps in the head from (a) Method 1 and (c) Method 5 and torso/breast model from (b) Method 1, and (d) Method 5